Automated Oscillator Macromodelling Techniques for Capturing Amplitude Variations and Injection Locking

Xiaolue Lai and Jaijeet Roychowdhury
Department of Electrical and Computer Engineering
University of Minnesota
Email: {laixl, jr}@ece.umn.edu

***Abstract*— We present a method for extracting comprehensive amplitude and phase macromodels of oscillators from their circuit descriptions. The macromodels are based on combining a scalar, nonlinear phase equation with a small linear time-varying system to capture slowly-dying amplitude variations. The comprehensive macromodels are able to correctly predict oscillator response in the presence of interference at far lower computational cost than that of full SPICE-level simulation. We also present an efficient numerical method for capturing injection locking in oscillators, thereby improving on the classic technique of Adler [1] in terms of accuracy and applicability to any kind of oscillator. We demonstrate the proposed techniques on LC and ring oscillators, comparing results from the macromodels against full SPICE-like simulation. Numerical experiments demonstrate speedups of orders of magnitude, while retaining excellent accuracy.**

I. Introduction

Oscillators are critical components of electronic and optical systems. They are often used, for example, for frequency-translation of information signals in communication systems. Phase-locked loops (PLLs), widely used in both digital and analog circuits for clock generation and recovery, frequency synthesis, *etc.*, feature voltage-controlled oscillators as key components. The design of oscillators and oscillator-based systems is an important part of overall system design; however, simulating oscillators presents unique challenges because of their fundamental property of neutral phase stability, often accompanied (especially in high-Q oscillators) with very slow amplitude responses that border on instability.

Traditional circuit simulators such as SPICE [11] consume significant computer time to simulate the transient behavior of oscillators. This is especially so for jitter simulation, since very small time-steps are required, and for many simulation cycles. As a result, specialized techniques based on using macromodels (*e.g.*, [2], [3], [7], [9], [10], [12]–[16]) have been developed for the simulation of oscillator-based systems. However, such approaches suffer from serious qualitative limitations. Most involve simple phase-integrating elements that do not capture amplitude variations, which can be important for second-order effects. An exception is the recent work of Vanassche et al [15], but even this involves linear phase integration, which (as we show in this paper) is qualitatively inadequate for predicting the important and fascinating phenomenon of *injection locking*. Moreover, Vanassche's method, developed using perturbation analysis of harmonic (LC) oscillators, is inapplicable to other topologies such as ring and relaxation oscillators which are widely used in digital systems, and increasingly, in high-performance mixed-signal systems as well.

In this paper, we present a method for constructing comprehensive oscillator macromodels, including both amplitude and phase characteristics, for any kind of oscillator regardless of operating mechanism. Our method, which is related to a rigorous nonlinear theory for oscillator phase noise [5], consists of an algorithm to extract amplitude and phase responses from an oscillator's circuit equations provided at, *e.g.*, the SPICE level. The macromodel produced is a combination of a scalar nonlinear differential equation [5] and a reduced linear time-varying system that is computationally simpler and of smaller size than the original oscillator, resulting in significant speedups in simulations. The macromodel approximates the totality of the output characteristics of the original oscillator circuit to perturbations well, and can be easily encapsulated in MATLAB/Simulink, Verilog-A, VHDL-AMS, *etc.*, for use in system-level simulation.

We provide comparisons of macromodels generated for LC and ring oscillators vs the original SPICE-level circuits, under different perturbation amplitudes and frequencies. Our numerical results demonstrate that the macromodels are able to reproduce the waveforms of SPICE-like simulation when the perturbation amplitude is under about 10% of the oscillator's load amplitude (this is considered large in most practical applications). Even with very small oscillators, we obtain speedups in the range of 1-2 orders of magnitude; much greater speedups are expected with larger circuits and more complex device models.

Further, we demonstrate the suitability of the nonlinear macromodel for predicting injection locking. Injection locking is a nonlinear dynamical phenomenon peculiar to oscillators, in which an oscillator's natural frequency changes to match that of a small injected perturbation. The phenomenon is universal to oscillators (manifesting itself, for example, as the synchronized flashing of fireflies, the locked swinging of grandfather clocks located close to each other, *etc.*) and has been increasingly used in recent years in novel, high-speed, oscillator designs.

Verifying the presence or absence of injection locking can be extremely difficult using SPICE-like simulations, especially for small injections at frequencies close to the oscillator's natural frequency (*i.e.*, the typical case). Existing approaches towards understanding and predicting injection locking are all directly based on Adler's classic 1946 paper [1], which provides a simplified quantitive explanation of the phenomenon for simple harmonic oscillators, leading to formulae for their lock range. Adler's approach is not general, being limited to LC harmonic oscillators and relying on analytical simplifications. Indeed, it requires the Q factor of the oscillator, therefore cannot be applied to, *e.g.*, ring oscillators, for which Q factors are not defined. In this paper, we apply the nonlinear macromodels mentioned above to develop an efficient numerical method for predicting injection locking. In addition to being generally applicable to all oscillators, our technique improves significantly on Adler's method, in terms of accuracy, even for LC oscillators.

The remainder of the paper is organized as follows. In Section II, we review nonlinear perturbation analysis of oscillators and the nonlinear phase macromodel. In Section III, we derive the oscillator amplitude macromodel. In Section IV, we apply the macromodel to predict injection locking, and in Section V, we present simulation results on three oscillator examples.

II. Nonlinear Perturbation Analysis

The standard approach for analyzing perturbed nonlinear systems is to linearize around an unperturbed trajectory. However, this approach does not suffice for analyzing oscillators. In [5], a novel phase macromodel based on nonlinear perturbation analysis was presented that is suitable for oscillators. Here, we first review the essentials of this approach.

A. Linear Perturbation Analysis

A general oscillator that is being perturbed can be described by

$$\dot{x} + f(x) = Bb(t), \tag{1}$$

where $b(t)$ is a perturbation applied to the free-running oscillator and $x(t)$ is a vector composed of the state variables of the oscillator. For

small perturbations, we can linearize (1) about its unperturbed orbit as

$$\begin{aligned}\dot{w}(t) \approx & -\frac{\partial f(x)}{\partial x}|_{x_s(t)} w(t) + Bb(t) \\ = & A(t)w(t) + Bb(t),\end{aligned} \tag{2}$$

where $w(t)$ represents deviations due to perturbations and $x_s(t)$ is the unperturbed steady-state solution of the oscillator. The periodic time-varying linear system (2) can be solved using Floquet theory [8] to obtain an expression for its state transition matrix

$$\Phi(t,\tau) = U(t)\exp(D(t-\tau))V(\tau). \tag{3}$$

$U(t)$ and $V(t)$ are T-periodic nonsingular matrices, satisfying biorthogonality conditions $v_i^T(t)u_j(t) = \delta_{ij}$, and $D = diag[\mu_1, ..., \mu_n]$, where μ_i are the Floquet exponents. As shown in [5], one of the Floquet exponents must be 0, and $\dot{x}_s(t)$ is one of the solutions of $w(t) = A(t)w(t)$, the homogenous part of (2).

Without loss of generality, we choose $\mu_1 = 0$ and $u_1(t) = \dot{x}_s(t)$. The *perturbation projection vector* (PPV) $v_1(t)$ satisfies $v_1^T(t)u_1(t) = 1$ [5], [6]. The PPV, which can be thought of as representing the oscillator's phase sensitivity to perturbations, is a periodic vector waveform with period identical to that of the unperturbed oscillator.

The particular solution of (2) is given by

$$w(t) = \sum_{i=1}^{n} u_i(t) \int_0^t \exp(\mu_i(t-\tau)) v_i^T(\tau) Bb(\tau) d\tau, \tag{4}$$

where $\mu_1 = 0$. A small perturbation $b(t)$ with the same frequency as $v_1(t)$ can always be chosen to satisfy that $v_i^T(t)Bb(t)$ has a nonzero average value; hence $w(t)$ can be made to grow unboundedly with t, in spite of $b(t)$ always remaining small. This contradicts the basic assumption for perturbation analysis, *i.e.*, that $w(t)$ is always small.

B. Nonlinear Phase Macromodel

To resolve this contraction, a key innovation of [5] was to rewrite (1) with the perturbation $Bb(t)$ split into two parts

$$\dot{x} + f(x) = b_1(t) + \tilde{b}(t), \tag{5}$$

where

$$b_1(t) = v_1^T(t + \alpha(t))Bb(t)u_1(t + \alpha(t)) \tag{6}$$

was shown to induce *only phase deviations* to the unperturbed system, while

$$\tilde{b}(t) = \sum_{i=2}^{n} v_i^T(t + \alpha(t))Bb(t)u_i(t + \alpha(t)) \tag{7}$$

was shown to contribute orbital deviations. The solution of $\dot{x} + f(x) = b_1(t)$ is in fact given by

$$x_p(t) = x_s(t + \alpha(t)), \tag{8}$$

where $\alpha(t)$ is the phase deviation due to the perturbation $b_1(t)$. Indeed, it can be shown [5] that $\alpha(t)$ is governed by the nonlinear differential equation

$$\dot{\alpha}(t) = v_1^T(t + \alpha(t)) \cdot Bb(t). \tag{9}$$

With the PPV $v_1(t)$ available for a given oscillator, its phase deviations due to perturbations can be efficiently evaluated by solving the one-dimensional nonlinear equation (9). Effective methods are available for computing the PPV from a SPICE-level description of the oscillator [5], [6] in either time or frequency domains.

In (9), $\alpha(t)$ has units of time; the phase deviation in radians is easily obtained by multiplying it with the free running oscillation frequency ω_0.

III. Amplitude Macromodel

The key utility of the decomposition (5) is that the orbital deviation does not grow unboundedly if only the $\tilde{b}(t)$ component of $b(t)$ is applied; hence, validity of small-signal perturbation analysis is restored, provided it is performed around the dynamically phase-shifted steady state $x_p(t) = x_s(t + \alpha(t))$ for it. Given an oscillator system

$$\dot{x} + f(x) = Bb(t), \quad y(t) = C^T x(t), \tag{10}$$

with solution

$$x(t) = x_p(t) + o(t), \tag{11}$$

(where $x_p(t) = x_s(t + \alpha(t))$, and $o(t)$ represents the orbital deviations due to the perturbation $\tilde{b}(t)$), (10) can be expressed as

$$\dot{x}_p(t) + \dot{o}(t) + f(x_p(t) + o(t)) = b_1(t) + \tilde{b}(t). \tag{12}$$

Linearizing (12) around $x_p(t)$, the orbital deviation $o(t)$ is given by

$$\begin{aligned}\dot{o}(t) \approx & -\frac{\partial f}{\partial x}|_{x_s(t+\alpha(t))} o(t) + \tilde{b}(t) \\ = & A(x_s(t + \alpha(t)))o(t) + \tilde{b}(t).\end{aligned} \tag{13}$$

Since $A(x_s(t + \alpha(t)))$ is not periodic, Floquet theory cannot be applied directly to analyze the linearized system. The transformation $\hat{t}(t) = t + \alpha(t)$ is therefore applied and $\hat{o}(\hat{t}) = o(t)$ and $\hat{\tilde{b}}(\hat{t}) = \tilde{b}(t)$ defined. (13) can then be rewritten as

$$\frac{d\hat{o}(\hat{t})}{dt} = A(x_s(\hat{t}))\hat{o}(\hat{t}) + \hat{\tilde{b}}(\hat{t}), \tag{14}$$

or,

$$(1 + \dot{\alpha}(t))\dot{\hat{o}}(\hat{t}) = A(x_s(\hat{t}))\hat{o}(\hat{t}) + \hat{\tilde{b}}(\hat{t}). \tag{15}$$

$\dot{\alpha}(t) = v_1^T(t)b_1(t) \ll 1$ since the perturbation $b_1(t)$ is assumed small. Dividing (15) by $1 + \dot{\alpha}(t)$ and Taylor expanding, we have

$$\dot{\hat{o}}(\hat{t}) = A(x_s(\hat{t}))\hat{o}(\hat{t}) + \hat{\tilde{b}}(\hat{t}) + R(\hat{t}), \tag{16}$$

where $R(\hat{t}) = v_1^T(\hat{t})\hat{b}(\hat{t})(A(x_s(\hat{t}))\hat{o}(\hat{t}) + \hat{\tilde{b}}(\hat{t}))$ is a quadratic term which is dropped, keeping only the linearized terms. The orbital deviation can then be expressed as a linear time-varying (LTV) system

$$\dot{\hat{o}}(\hat{t}) = A(x_s(\hat{t}))\hat{o}(\hat{t}) + \hat{\tilde{b}}(\hat{t}). \tag{17}$$

This linear system has the same form as (2), so its solution can be expressed as

$$\hat{o}(\hat{t}) = \sum_{i=1}^{n} u_i(\hat{t}) \int_0^{\hat{t}} \exp(\mu_i(\hat{t} - \tau)) v_i^T(\tau) \hat{\tilde{b}}(\tau) d\tau. \tag{18}$$

From (7), it is clear that $\hat{\tilde{b}}(\hat{t})$ contains no u_1 component, so the $i = 1$ term in (18) can be dropped; the u_1 component, in fact, results in the grown phase deviation $\alpha(t)$. Hence, $\hat{\tilde{b}}(\hat{t})$ can be replaced by $B\hat{b}(\hat{t})$ in (18), and $o(t)$ is given by

$$o(t) = \hat{o}(\hat{t}) = \sum_{i=2}^{n} u_i(\hat{t}) \int_0^{\hat{t}} \exp(\mu_i(\hat{t} - \tau)) v_i^T(\tau) B\hat{b}(\tau) d\tau, \tag{19}$$

where $\hat{t} = t + \alpha(t)$ and $\hat{b}(\hat{t}) = b(t)$. The output of the oscillator can therefore be expressed as

$$y(t) = C^T x_s(\hat{t}) + \sum_{i=2}^{n} C^T u_i(\hat{t}) \int_0^{\hat{t}} \exp(\mu_i(\hat{t} - \tau)) v_i^T(\tau) B\hat{b}(\tau) d\tau, \tag{20}$$

with the *amplitude deviation* being

$$\hat{A}(\hat{t}) = \sum_{i=2}^{n} C^T u_i(\hat{t}) \int_0^{\hat{t}} \exp(\mu_i(\hat{t} - \tau)) v_i^T(\tau) B\hat{b}(\tau) d\tau. \tag{21}$$

To develop a reduced macromodel that captures only the important amplitude components, we define the weighted factor $w_i(t)$ for each Floquet exponent μ_i to be

$$w_i(t) = C^T u_i(t) \exp(\mu_i T) v_i^T(t) B. \tag{22}$$

A large $w_i(t)$ implies that the corresponding Floquet exponent will have a large contribution to the amplitude deviation. Hence, $w_i(t)$ can be evaluated for each Floquet exponent, and exponents with small weights can be dropped to obtain a reduced diagonal matrix $\bar{D}$. If a Floquet exponent μ_i is dropped, the corresponding $u_i(t)$ and $v_i(t)$

are also dropped, resulting in a reduced matrices, $\bar{U}(t)$ and $\bar{V}(t)$. On completing this process, a reduced system for the amplitude deviation $A(t)$

$$\hat{A}(\hat{t}) \approx C^T \bar{U}(t) \int_0^{\hat{t}} \exp(\bar{D}(\hat{t}-\tau))\bar{V}(\tau)B\hat{b}(\tau)d\tau \tag{23}$$

is obtained. This can be expressed as a macromodel in ODE form as

$$\begin{aligned} \dot{\hat{a}}(\hat{t}) &= \bar{D}\hat{a}(\hat{t}) + \bar{V}(\hat{t})Bb(t), \\ A(t) &= \hat{A}(\hat{t}) = C^T\bar{U}(\hat{t})\hat{a}(\hat{t}), \end{aligned} \tag{24}$$

where $\bar{D} = diag[\breve{\mu}_1, ..., \breve{\mu}_m]$, $\bar{U}(\hat{t}) \in R^{n\times m}$, $\bar{V}(\hat{t}) \in R^{m\times n}$ and m is the size of the reduced system.

Combining the nonlinear phase equation (9) with the above amplitude macromodel, a comprehensive macromodel is obtained. The flow of the macromodelling process is outlined below:

1) Obtain the steady state $x_s(t)$.
2) Calculate $U(t)$, $V(t)$ and Floquet exponents using numerical methods [4]–[6].
3) Solve (9) for the phase deviation $\alpha(t)$.
4) Solve (24) for the amplitude deviation $A(t)$.
5) The output of the oscillator is given by

$$y(t) = C^T x_s(\hat{t}) + \hat{A}(\hat{t}). \tag{25}$$

IV. Predicting Injection Locking

Injection locking is a nonlinear dynamical phenomenon occurring in all oscillators. When an oscillator is perturbed by a weak external signal close to its free-running frequency, the oscillator's frequency changes to become identical to that of the perturbing signal. Capturing injection locking using traditional simulation presents challenges. SPICE-level simulation of oscillators is usually inefficient, since oscillators often require thousands of cycles to lock to an injecting signal, with each simulation cycle requiring large numbers of very small timesteps for acceptable phase accuracy. If the frequency of the injected signal is close to oscillator's free-running frequency, it also becomes very difficult to distinguish injection locking from observing time-domain waveforms.

A. The Adler Equation

In [1], Adler derived the following equation for the instantaneous beat frequency of LC tanks oscillators perturbed by an external signal:

$$\frac{d\alpha}{dt} = -\frac{V_{inj}}{V_0}\frac{\omega_0}{2Q}\sin(\alpha) + \Delta\omega_0, \tag{26}$$

where V_0 and ω_0 are the output voltage and frequency of the unperturbed oscillator and $\frac{d\alpha}{dt}$ is the instantaneous beat frequency. $\Delta\omega_0$ is the frequency difference, which satisfies $\frac{\Delta\omega_0}{\omega_0} \ll \frac{1}{2Q}$. When the oscillator locks to the external injection signal, the beat frequency vanishes, resulting in the *locking condition*

$$\sin(\alpha) = 2Q\frac{V_0}{V_{inj}}\frac{\Delta\omega_0}{\omega_0}. \tag{27}$$

Since the values of $\sin(\alpha)$ can only be between -1 and $+1$, the maximum locking range of the oscillator is given by

$$\frac{V_{inj}}{V_0} > 2Q|\frac{\Delta\omega_0}{\omega_0}|. \tag{28}$$

Adler's equation is widely used for capturing injection locking in oscillators. However, it suffers from an immediate limitation: it requires a LC-tank Q factor for (28). For oscillators that rely on abruptly switching elements, *e.g.*, ring or relaxation oscillators, Adler's equation is of limited utility. Furthermore, even for LC oscillators, the predictive ability of Adler's equation is typically limited to a range of Q values.

B. Using the Nonlinear Phase Macromodel for Injection Locking

The nonlinearity of the phase macromodel (9) makes it well suited for capturing injection locking effects in any oscillator for which the PPV is available. If the oscillator locks to an injected signal, the oscillator's phase follows that of the injected signal; this leads to the relationship

$$\omega_0 t + \phi(t) = \omega_1 t + \theta, \text{ or } \quad \phi(t) = (\omega_1 - \omega_0)t + \theta, \tag{29}$$

where ω_0 is the frequency of the free-running oscillator, ω_1 is the frequency of the injected signal, $\phi(t)$ is the phase deviation of the perturbed oscillator, and θ is a constant which represents the phase difference between the locked oscillator and the injected signal. It is clear from (29) that if the oscillator locks to the injected signal, the phase shift due to the injected signal should grow with time linearly with a slope of $\omega_1 - \omega_0$. Since $\alpha(t)$ has units of time, the phase deviation in radians can be expressed as

$$\phi(t) = \omega_0\alpha(t). \tag{30}$$

Substituting (30) into (29), we have

$$\omega_0\alpha(t) = (\omega_1 - \omega_0)t + \theta, \text{ or } \quad \alpha(t) = \frac{\Delta\omega_0}{\omega_0}t + \frac{\theta}{\omega_0}, \tag{31}$$

where $\Delta\omega_0 = \omega_1 - \omega_0$ is the frequency difference between the free-running oscillator and the injected signal. This relationship provides a direct means to check for locking behavior in oscillators. For example, if an oscillator is injected with a signal with frequency 10% higher than its free-running frequency, using (31), the oscillator locks to the signal if its phase shift $\alpha(t)$ increases linearly with a slope of 0.1.

Substituting (31) into the nonlinear phase equation (9), we have

$$\begin{aligned} \frac{\Delta\omega_0}{\omega_0} &= v_1(t + \frac{\Delta\omega_0 t + \theta}{\omega_0})A_{inj}\sin(\omega_1 t) \\ &= v_1(\frac{\omega_1 t + \theta}{\omega_0})A_{inj}\sin(\omega_1 t), \end{aligned} \tag{32}$$

where A_{inj} is the amplitude of the injection signal and θ is the phase difference between the injection signal and the oscillator's output. Since $v_1(t)$ has the same frequency as the free running oscillator, the frequency of $v_1(\frac{\omega_1}{\omega_0}t)$ must equal the injection frequency ω_1. As $\Delta\omega_0$ in (32) increases, the nonlinear locking mechanism changes the locked phase difference θ to match the slope $\frac{\Delta\omega_0}{\omega_0}$. Since (32) is T_1-periodic, integrating both sides for one period of T_1 leads to

$$\int_0^{T_1} \frac{\Delta\omega_0}{\omega_0}dt = \int_0^{T_1} v_1(\frac{\omega_1 t + \theta}{\omega_0})A_{inj}\sin(\omega_1 t)dt \tag{33}$$

or

$$\frac{\Delta\omega_0}{\omega_0} = \frac{A_{inj}}{T_1}\int_0^{T_1} v_1(\frac{\omega_1 t + \theta}{\omega_0})\sin(\omega_1 t)dt. \tag{34}$$

Hence, the maximum locking range is given by

$$|\frac{\Delta\omega_0}{\omega_0}| < \eta A_{inj}, \tag{35}$$

where

$$\begin{aligned} \eta &= \max_{\theta=0\to 2\pi}(\frac{1}{T_1}\int_0^{T_1} v_1(\frac{\omega_1 t + \theta}{\omega_0})\sin(\omega_1 t))dt \\ &= \max_{t_0=0\to 1}(\int_0^1 v_1(\frac{t+t_0}{f_0}))\sin(2\pi t)dt. \end{aligned} \tag{36}$$

η is independent of the injection frequency f_1, and can be easily calculated by numerical methods if the PPV is available. Note that (36) has a form similar to the Adler equation. Unlike Adler's equation, however, it can apply to any physical oscillator, regardless of operating mechanism; indeed, the underlying ideas used to derive (36) appear quite different from Adler's.

V. Numerical Results

In this section, we apply and validate the techniques presented above for capturing phase/amplitude variations and injection locking, using LC and ring oscillators. All simulations were performed using **MATLAB** on a Linux machine with an AMD Athlon -2200+ processor. In what follows, we predict amplitude deviations and injection

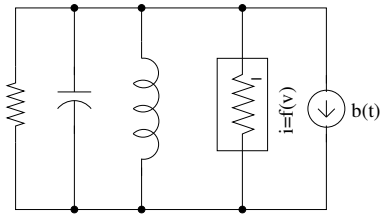

Fig. 1. A simple LC oscillator.

locking of oscillators using our macromodels, and compare the results with SPICE-like simulations of the full oscillator circuit in the same **MATLAB** environment. For injection locking analysis, we plot the relationship between injection amplitude and maximum locking range using full simulation and compare with the results by evaluating (35). These experiments demonstrate that our macromodels work very well when the amplitude of the perturbation is less than about 10% of the oscillator's working load. Speedups of 30–100 times are obtained using the macromodels.

A. 1GHz LC oscillator

Figure 1 depicts the block diagram of a simple LC oscillator, whose differential equations are

$$\begin{aligned} -C\frac{d}{dt}v(t) &= \frac{v(t)}{R} + i(t) + S\tanh\left(\frac{G_n}{S}v(t)\right) + b(t) \\ L\frac{d}{dt}i(t) &= v(t). \end{aligned} \tag{37}$$

$L = 4.869\times10^{-7}/(2\pi)\ H$, $C = 2\times10^{-12}/(2\pi)\ F$, $R = 100\ \Omega$, $S = 1/R$ and $G_n = -1.1/R$. With these parameters, the LC tank has a resonance frequency of 1 GHz, and the inductor current has amplitude $A_0 = 1.2$mA.

1) Phase and amplitude macromodel: Since the simple LC oscillator has only two unknowns, the corresponding system has two Floquet exponents. So this is a minimum system, and it cannot be reduced any more. However, using our macromodel, we get a linear equation for amplitude and a mildly nonlinear equation for phase deviation. Both of them can be simulated with much larger timesteps. A key feature of the macromodel is that these two equations are independent and can be solved separately without matrix computations. In our simulation, the runtime using the full circuit transient simulation takes 230 seconds for a simulation time of 200 cycles. However, it takes only 8 seconds to simulate the same number of cycles using the macromodel, representing a 29 times speedup. Moreover, as the original system's size increases, larger speedups are obtained.

First, we investigate the response of the LC oscillator under a small impulse perturbation injected at steady state. The amplitude of the impulse is 0.2mA and its duration is 10% of the period. Comparisons of results from the macromodels and the full SPICE-level simulation are shown in Figure 2. As can be seen, there is an excellent match in both phase and amplitude characteristics.

Now we inject a sinusoidal signal to the LC oscillator. The injection amplitude is 5% of the oscillator's load amplitude, and the injection frequency is $1.03f_0$, where f_0 is the oscillator's free running frequency. Results from a simulation of 100 cycles are shown in Figure 3(a) (phase deviations) and Figure 3(b) (amplitude deviations). From the phase and amplitude information obtained from simulating the macromodel, voltage and current waveforms are re-constructed using (25) and shown in Figure 3(c). Comparing these against SPICE-level transient simulations of the original circuit (shown in Figure 3(d)), the match is observed to be very close. A more detailed comparison of 15 cycles (from $t = 25T$ to $t = 40T$) is shown in Figure 4.

To test the range of validity of our macromodel with respect to the amplitude of input perturbations, we increase the injection amplitude gradually, and plot the results in Figure 5. The macromodel works well when the injection strength is less than about 10% of A_0. When

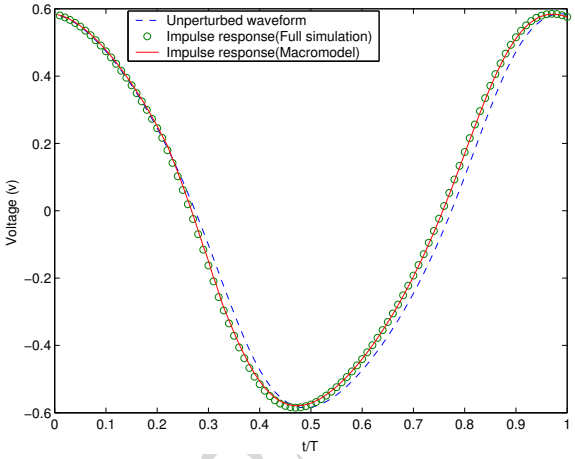

Fig. 2. Phase and amplitude deviations under impulse perturbation.

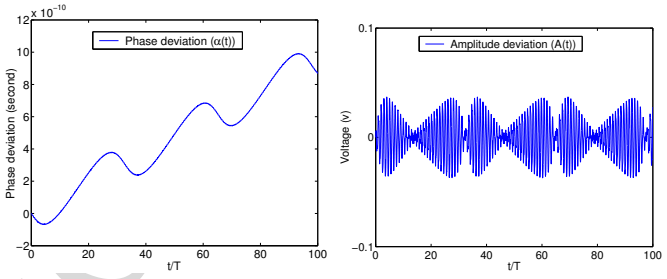

(a) Phase deviation

(b) Amplitude deviation

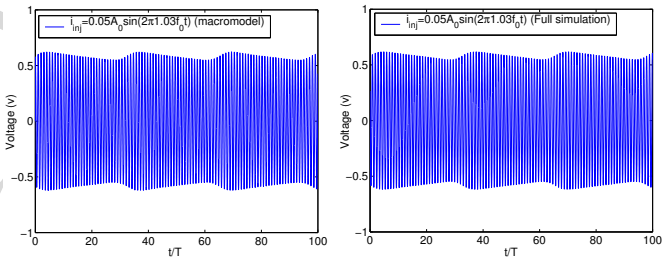

(c) Oscillator output (macromodel)

(d) Oscillator output (full simulation)

Fig. 3. Output of the simple LC oscillator under the perturbation $i_{inj} = 0.05A_0\sin(1.03\omega_0 t)$.

the injection amplitude increases, the macromodel's prediction error increases, resulting in a higher beat frequency. When the injection amplitude increase to $0.25A_0$, the oscillator locks to the external signal, but at these extremely high injection levels, the macromodel fails to capture lock correctly, because of its underpinnings in small-signal linearization. Such high injections are usually rare in practice and do not significantly limit the applicability of our macromodels.

2) Injection Locking Analysis: (35) reveals a linear relationship between the injection amplitude A_{inj} and the frequency difference $\Delta\omega_0$; given the PPV, the slope η in (35) can be calculated using (36). Figure 6 shows the locking range of the LC oscillator. The nonlinear phase macromodel can capture injection locking well when the injection amplitude is below 15% of A_0. η, which can be calculated very quickly (in a few seconds), can be used to predict injection locking by evaluating (35). In contrast, full SPICE-like simulation requires four minutes to predict locking on this low-Q oscillator. η

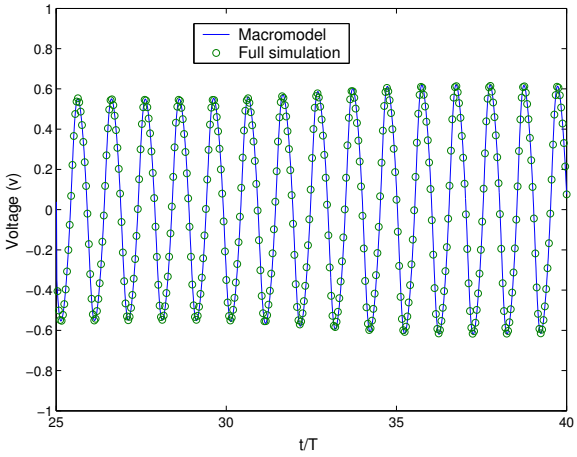

Fig. 4. Output of the simple LC oscillator under the perturbation $i_{inj} = 0.05A_0 \sin(1.03\omega_0 t)$.

needs to be calculated only once; it can then be reused to investigate injection locking under different injection frequencies and strengths. A similar feature is not available when solving the full system of equations. Furthermore, when the Q-factor of the LC oscillator is made high, thousands of cycles elapse before lock. The simulation time for the full circuit becomes more than one hour on our system, while that for the macromodel remains unchanged.

B. Three-Stage Ring Oscillator

Figure 7 depicts the block diagram of a three-stage ring oscillator, described by the differential equations

$$\begin{aligned} -C_1 \frac{d}{dt} v_1(t) &= \frac{v_1}{R1} - \frac{\tanh(G_{m3} v_3(t))}{R_1} \\ -C_2 \frac{d}{dt} v_2(t) &= \frac{v_2}{R2} - \frac{\tanh(G_{m1} v_1(t))}{R_2} \\ -C_3 \frac{d}{dt} v_3(t) &= \frac{v_3}{R3} - \frac{\tanh(G_{m2} v_2(t))}{R_3}. \end{aligned} \tag{38}$$

Each stage of this ring oscillator is identical, we have $C_1 = C_2 = C_3 = 2nF$, $R_1 = R_2 = R_3 = 1k\Omega$, and $G_{m1} = G_{m2} = G_{m3} = -5$. The oscillator has a natural frequency of 153498Hz and a maximum load current of $A_0 = 1.2$mA.

1) Phase and amplitude macromodel: This oscillator has the system size of 3, so it has two Floquet exponents for amplitude macromodel. In the following, we simulate two macromodels: a reduced macromodel retaining only the dominant Floquet exponent, and a "full" macromodel, which keeps both Floquet exponents. Our numerical experiments below reveal very little difference between the two macromodels, indicating that size reduction leads to insignificant loss of accuracy. Both macromodels match full SPICE-level simulation well, and deliver about a 30 times speedup.

First, we apply a perturbation current with amplitude $A_{inj} = 0.05A_0$ and frequency $f_{inj} = 1.04f_0$ to the oscillator, and simulate it for 100 cycles. Figure 8(b) and Figure 8(c) depict the results of the reduced macromodel and the full macromodel. Both waveforms match full simulation well, as shown in Figure 8(d). Increasing the injection amplitude gradually, we show the changes that occur in amplitude and phase response in Figure 9. We obtain a trend similar to that for the LC oscillator: the macromodels work well when the injection amplitude is less than about 10% of A_0.

2) Injection locking analysis: As mentioned earlier, a key advantage of our approach is its general applicability for predicting injection locking. Using (36), the maximum locking range of this ring oscillator is easily predicted, as plotted in Figure 10. As before, locking is predicted well when the injection amplitude is below about 10% of A_0. For this case, η is calculated in several seconds, while full SPICE-like simulation requires five minutes to capture locking.

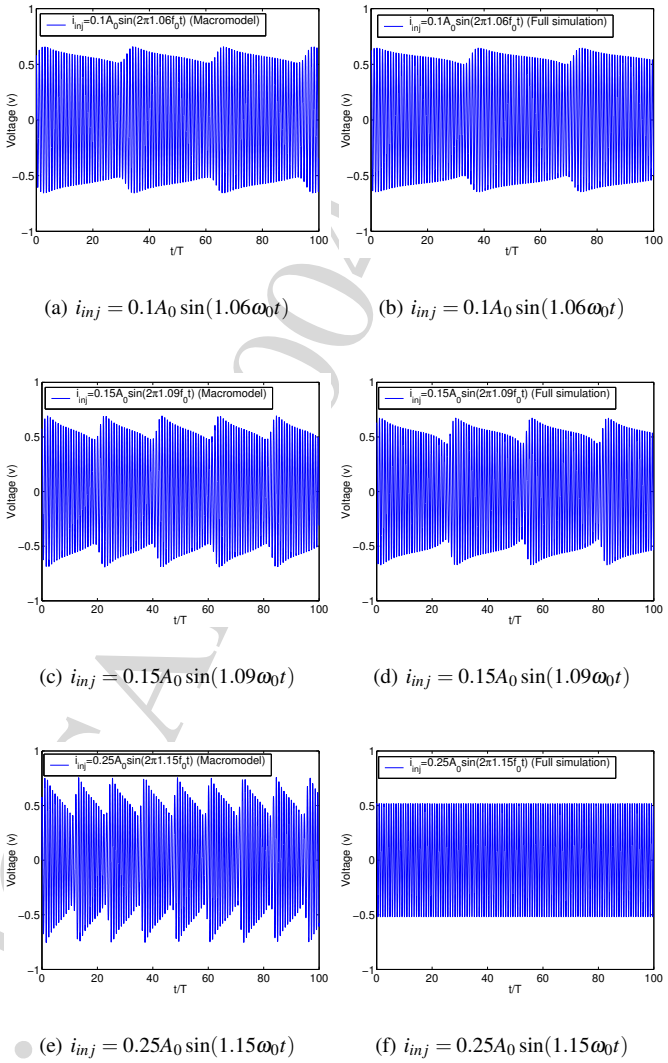

(a) $i_{inj} = 0.1A_0 \sin(1.06\omega_0 t)$ (b) $i_{inj} = 0.1A_0 \sin(1.06\omega_0 t)$

(c) $i_{inj} = 0.15A_0 \sin(1.09\omega_0 t)$ (d) $i_{inj} = 0.15A_0 \sin(1.09\omega_0 t)$

(e) $i_{inj} = 0.25A_0 \sin(1.15\omega_0 t)$ (f) $i_{inj} = 0.25A_0 \sin(1.15\omega_0 t)$

Fig. 5. Outputs of the simple LC oscillator under different perturbations.

C. 4GHz LC Oscillator

The circuit and parameters of another LC oscillator are shown in Figure 11. The oscillator has a free-running frequency of about 4GHz, and the inductor current through L_1 has an oscillation amplitude of 15mA.

1) Phase and amplitude macromodel: The size of the LC oscillator system is 6. We find, somewhat surprisingly, that an amplitude macromodel of size only 1 captures the oscillator's dynamics very well. With only a one-dimensional nonlinear phase equation and a one-dimensional amplitude equation against a 6-dimensional full oscillator circuit, large speedups (more than 100 times) are obtained.

Injecting a voltage perturbation in series with the inductor L_1 and simulating under different perturbation strengths, we obtain the results shown in Figure 12. When the perturbation amplitude is 2mV, the amplitude deviation due to this perturbation is about 1mA, which is 6% of the inductor's oscillation current. The macromodel matches full simulation well at this perturbation level, as shown in Figure 12(a) and Figure 12(b). As the injection amplitude grows to $8mV$, the amplitude deviation increases to $4mA$, which is about 25% of the inductor's oscillation current. The macromodel can still predict beats in the waveform well; however, the shape of the waveform is no longer as accurate, as shown in Figure 12(e) and Figure 12(f).

2) Injection locking analysis: Using (36) to calculate the slope η provides quick prediction of injection locking, as in the previous

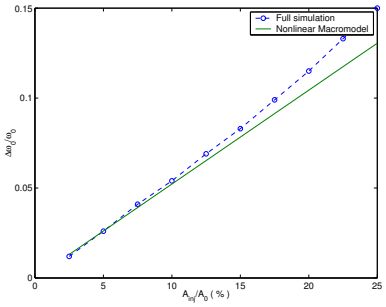

(a) Injection frequency is higher than the oscillator's frequency

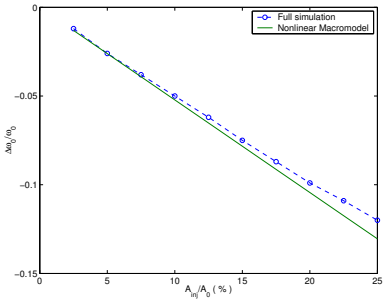

(b) Injection frequency is lower than the oscillator's frequency

Fig. 6. Locking range of the simple LC oscillator.

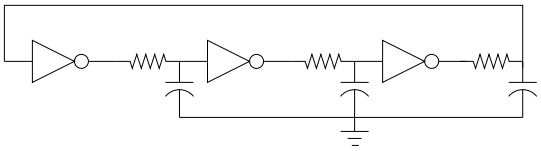

Fig. 7. A three-stage ring oscillator.

cases. Comparing against full SPICE-level simulation with different injection amplitudes in Figure 13, it is evident that the macromodel's results match full simulation very well, especially when the injection amplitude is less than 40mV.

VI. Conclusions

We have presented a novel technique to extract simple amplitude/phase macromodels from detailed circuit descriptions of any physical oscillator. The macromodels are able to predict oscillator phase and amplitude deviations well in the presence of perturbations and offer significant speedups over full SPICE-like simulation. We have demonstrated the use of these macromodels for capturing injection locking in oscillators, a feature that eludes oscillator macromodels in common industrial use today. Our injection-locking technique generalizes and overcomes limitations of the classic Adler equation. Numerical results demonstrate the ability of the macromodels to predict the totality of oscillators responses well, while providing large speedups over full SPICE-level simulation. We are currently developing efficient, Krylov-subspace-based variants of our method that will be applicable to large systems, resulting in macromodels that are expected to yield speedups of 3 or more orders of magnitude with insignificant loss of accuracy.

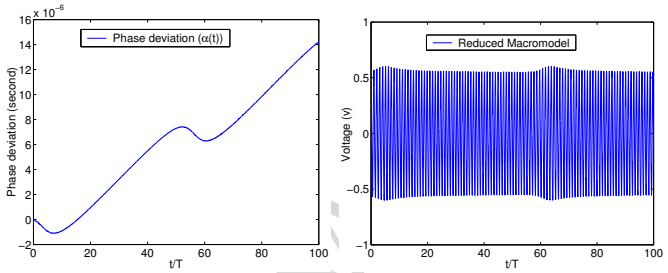

(a) Phase deviation

(b) Oscillator output (reduced macromodel)

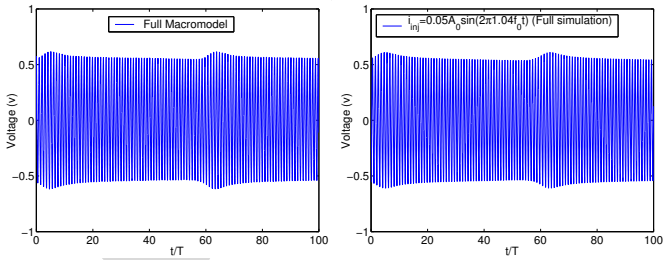

(c) Oscillator output (full macromodel)

(d) Oscillator output (full simulation)

Fig. 8. Output of the simple ring oscillator under the perturbation $i_{inj} = 0.05A_0 \sin(1.04\omega_0 t)$.

References

[1] R. Adler. A study of locking phenomena in oscillators. *Proceedings of the I.R.E. and Waves and Electrons*, 34:351–357, June 1946.

[2] A. Costantini, C. Florian, and G. Vannini. Vco behavioral modeling based on the nonlinear integral approach. *IEEE International Symposium on Circuits and Systems*, 2:137–140, May 2002.

[3] A. Demir, E. Liu, A.L. Sangiovanni-Vincentelli, and I. Vassiliou. Behavioral simulation techniques for phase/delay-locked systems. In *Proceedings of the Custom Integrated Circuits Conference 1994*, pages 453–456, May 1994.

[4] A. Demir, D. Long, and J. Roychowdhury. Computing phase noise eigenfunctions directly from steady-state jacobian matrices. In *IEEE/ACM International Conference on Computer Aided Design*, pages 283–288, November 2000.

[5] A. Demir, A. Mehrotra, and J. Roychowdhury. Phase noise in oscillators: a unifying theory and numerical methods for characterization. *IEEE Trans. on Circuits and Systems-I:Fundamental Theory and Applications*, 47(5):655–674, May 2000.

[6] A. Demir and J. Roychowdhury. A reliable and efficient procedure for oscillator ppv computation, with phase noise macromodelling applications. *IEEE Trans. on Computer-Aided Design of Integrated Circuits and Systems*, 22(2):188–197, February 2003.

[7] M. Gardner. *Phase-Lock Techniques*. Wiley, New York, 1966.

[8] R. Grimshaw. *Nonlinear Ordinary Differential Equations*. Blackwell Scientific, New York, 1990.

[9] A. Hajimiri and T.H. Lee. A general theory of phase noise in electrical oscillators. *IEEE Journal of Solid-State Circuits*, 33(2), February 1998.

[10] M. F. Mar. An event-driven pll behavioral model with applications to design driven noise modeling. In *Proc. Behav. Model and Simul.(BMAS)*, 1999.

[11] L. Nagel. *SPICE2: A Computer Program to Simulate Semiconductor Circuits*. Electron. Res. Lab., Univ. Calif., Berkeley, 1975.

[12] O. Narayan and J. Roychowdhury. Multi-time simulation of voltage-controlled oscillators. In *IEEE Proc. Design Automation Conf.*, pages 629–634, June 1999.

[13] E. Ngoya and R. Larcheveque. Envelope transient analysis: A new method for the steady state analysis of microwave communication circuits and systems. In *IEEE Pro. Microwave Theory Tech. Symp. Digest*, pages 1365–1368, June 1996.

[14] M. Schwab. Determination of the steady state of an oscillator by a combined time-frequency method. *IEEE Trans. Microwave Theory Tech.*, 39:1391–1402, August 1991.

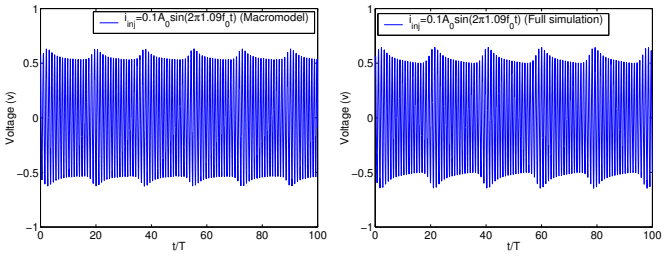

(a) $i_{inj} = 0.1A_0 \sin(1.09\omega_0 t)$ (b) $i_{inj} = 0.1A_0 \sin(1.09\omega_0 t)$

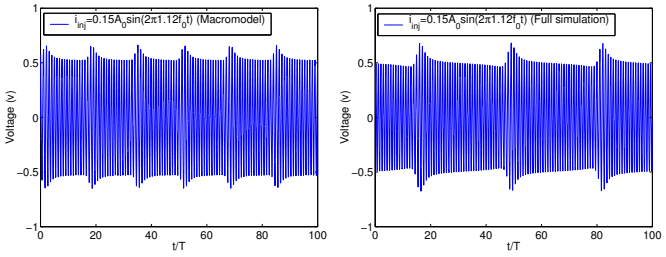

(c) $i_{inj} = 0.15A_0 \sin(1.12\omega_0 t)$ (d) $i_{inj} = 0.15A_0 \sin(1.12\omega_0 t)$

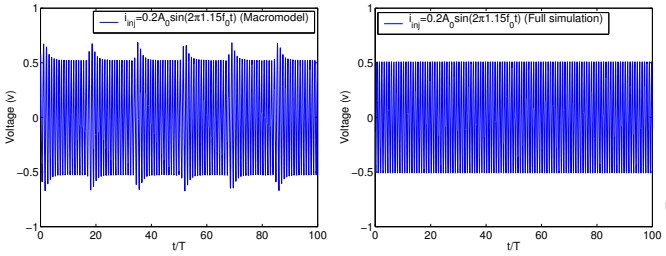

(e) $i_{inj} = 0.2A_0 \sin(1.15\omega_0 t)$ (f) $i_{inj} = 0.2A_0 \sin(1.15\omega_0 t)$

Fig. 9. Outputs of the simple ring oscillator under various perturbations.

[15] P. Vanassche, G.G.E. Gielen, and W. Sansen. Behavioral modeling of coupled harmonic oscillators. *IEEE Trans. on Computer-Aided Design of Integrated Circuits and Systems*, 22(8):1017–1026, August 2003.

[16] L. Wu, H.W. Jin, and W.C. Black. Nonlinear behavioral modeling and simulation of phase-locked and delay-locked systems. In *Proceedings of IEEE CICC, 2000*, pages 447–450, May 2000.

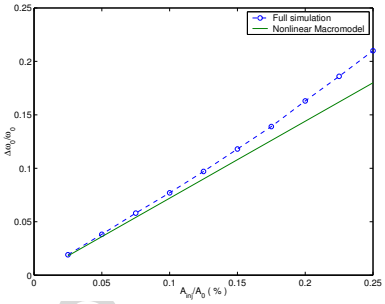

(a) Injection frequency is higher than the oscillator's frequency

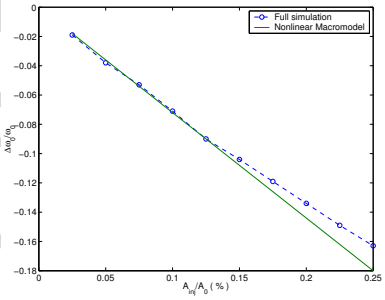

(b) Injection frequency is lower than the oscillator's frequency

Fig. 10. Locking range of the simple ring oscillator.

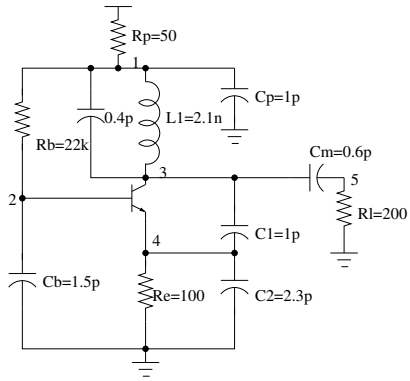

Fig. 11. A 4GHz LC oscillator.

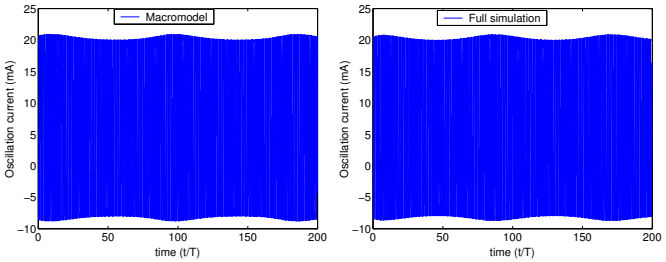

(a) $v_{inj} = 0.002\sin(1.012\omega_0 t)$ (b) $v_{inj} = 0.002\sin(1.012\omega_0 t)$

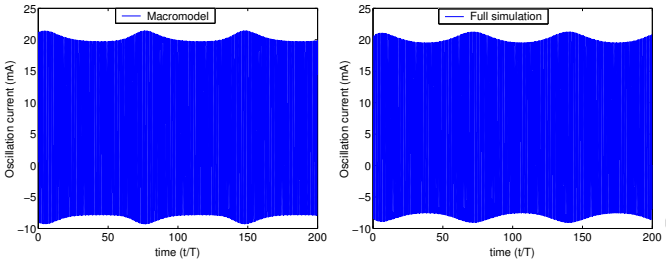

(c) $v_{inj} = 0.004\sin(1.016\omega_0 t)$ (d) $v_{inj} = 0.004\sin(1.016\omega_0 t)$

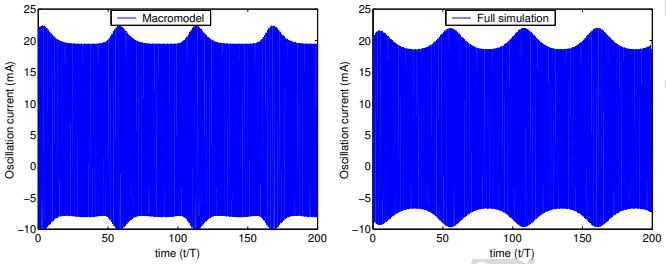

(e) $v_{inj} = 0.008\sin(1.024\omega_0 t)$ (f) $v_{inj} = 0.008\sin(1.024\omega_0 t)$

Fig. 12. Outputs of the 4GHz LC oscillator under different perturbations.

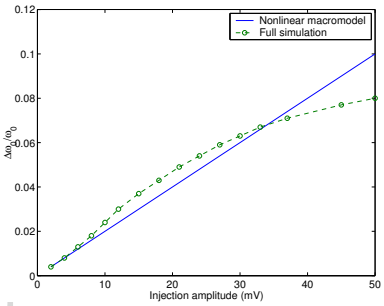

(a) Injection frequency is higher than the oscillator's frequency

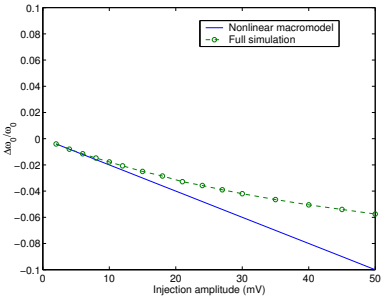

(b) Injection frequency is lower than the oscillator's frequency

Fig. 13. Locking range of the 4GHz LC oscillator.